

Ni incorporation in pSOFC anode ceramic matrix: Part I. Wet chemical reduction in an aqueous medium

M. Gabrovska^{1*}, D. Nikolova¹, E. Mladenova², D. Vladikova², S. Rakovsky¹, Z. Stoynov²

¹*Institute of Catalysis, Bulgarian Academy of Sciences, Acad. G. Bonchev Str., bl. 11, Sofia 1113, Bulgaria*

²*Acad. Evgeni Budevski Institute of Electrochemistry and Energy Systems, Bulgarian Academy of Sciences, Acad. G. Bonchev str., bl. 10, Sofia 1113, Bulgaria*

Received February 2, 2017 Revised March 11, 2017

Yttrium-doped barium cerate $\text{BaCe}_{0.85}\text{Y}_{0.15}\text{O}_{2.925}$ (BCY15) with ABO_3 perovskite-type structure was used as an anode ceramic matrix for the preparation of Ni-based BCY15 cermet anode for proton conducting solid oxide fuel cell (pSOFC). The possibility of metal nickel incorporation in BCY15 by wet-chemical reduction route in an aqueous medium with hydrazine was examined. Powder X-ray diffraction, N_2 -physisorption and SEM techniques were used for characterization of the synthesized BCY15/Ni powder. The electrochemical properties of Ni-based BCY15 anode cermet were determined by impedance spectroscopy after high-temperature sintering followed by reduction in hydrogen atmosphere. It was found that BCY15/Ni anode cermet demonstrated electrochemical performance similar to that of commercial NiO-based anode cermets in respect to the electronic conductivity of the Ni net. This makes the BCY15/Ni anode cermet suitable for application in BCY-based pSOFC. It may be concluded that the wet-chemical reduction route using hydrazine in an aqueous medium is a promising approach for incorporation of the metal nickel in the BCY15 anode ceramic matrix. This method provides better conditions for nickel introduction in the anode ceramic matrix in comparison with the classical solid state ceramic approach.

Key words: BCY15/Ni cermet anode, wet-chemical reduction by hydrazine, PXRD, electrochemical impedance spectroscopy.

INTRODUCTION

Solid oxide fuel cells (SOFCs) are one of the most efficient and environmental-friendly technologies available for generating power from hydrogen, natural gas, and other renewable fuels. SOFC is an all-ceramic device (two electrodes in contact with a dense ceramic electrolyte) that usually operates at elevated temperatures (800–1000°C) where it has sufficient conductivity, thus allowing internal reforming. It promotes rapid electro catalysis with non-precious metals and produces high quality heat by product for co-generation. Major drawbacks are connected to degradation phenomena occurring at high temperatures [1-3]. In this regard, fuel cells based on proton conductor electrolytes (pSOFC) are of great interest for their potential to operate at intermediate temperatures (400–600°C) thus alleviating the technological problems of SOFCs. Proton conductors are practicable electrolytes at intermediate temperatures because protons migrate more easily than oxygen ions at 400–600°C, thus conductivities are high enough for technical applications [4].

The oxygen-deficient ceramic oxides, in particular with perovskite type structure ABO_3 , are recognized as the most efficient materials that can be used as electrolytes or electrodes (metal-ceramic electrode structures) in pSOFCs, where the A site is occupied by an alkaline earth element, such as Ba, Sr, and Ca, while the B site is occupied by a tetravalent element, usually Ce or Zr. To promote protonic conductivity, it is paramount to dope the B-site with suitable trivalent elements, such as Y, Nd, Sm, Yb, In, Eu, Gd, etc. Doping with a trivalent element via the dissolution of hydroxyl ions at vacant oxygen sites induces the formation of oxygen vacancies, which play a crucial role in the formation of mobile protons [5, 6]. ABO_3 perovskite structured materials like Y-doped barium cerate ($\text{BaCe}_{1-x}\text{Y}_x\text{O}_{3-}$), commonly noted BCY, are of particular interest because they exhibit high proton conductivity, high electronic conductivity, and excellent chemical stability under reduced fuel cell environment over a wide temperature range. Thus, it could be considered as a promising proton conducting electrolyte for pSOFCs [3, 7-13]. BCY is a classical proton conducting electrolyte which may be exploited in two different functional layers of pSOFC: as proton conducting electrolyte and metal-cermet anode.

An inspection of the literature prompts that some metals can be used in SOFC anodes as

To whom all correspondence should be sent:
E-mail: margo@ic.bas.bg

catalysts for the fuel oxidation, as well as for ensuring electron conductivity, due to the reducing conditions of the fuel during fuel cell operation. The state-of-the-art metal for incorporation in the anode ceramic matrix is nickel. In pSOFC it is coupled with a protonic conducting ceramic to form the so called cermet. The selection of Ni is due to its excellent catalytic activity for hydrogen oxidation in the intermediate temperature range and high electrical conductivity. Ni has performance similar to that of the precious metal-based catalysts, thus, offering significant cost savings [14, 15]. To ensure sufficient current collection, the nickel content is usually over 35 vol. % to form a percolation path for electron transport [16]. The presence of proton conducting ceramic matrix in the anode composite improves the electrode performance, providing a conductivity network for H^+ ions, thus extending the triple-phase boundary (TPB) length [15].

It is well known that the preparative route plays a critical role on the physical and chemical properties of the reaction products, controlling the structure, morphology, grain size and surface area of the obtained materials. Traditionally, anode cermets are prepared by the standard ceramic technology from mixture of their constituent oxides in the so called solid state reaction or “shake and bake”. High temperature is a must in order to accelerate the slow solid–solid diffusion [17]. As a result of the low kinetics and high temperature, this costly method yields solids with low homogeneity, often presence of undesired secondary phases and uncontrolled (and typically large) particle size of low surface area [18].

Alternative approaches are wet chemical synthetic methods which permit mixing of the elements in liquid media at the atomic level resulting in lower firing temperatures, controlled particle size, morphology and improved surface area. Hydrazine is attractive reducing agent for the preparation of fine nickel powder due to its strong reduction properties in low temperature range and high pH values [19]. The temperature and pH dependence of hydrazine reducing ability makes the synthesis easily controllable [19, 20].

In this study, a wet chemical approach for Ni introduction in the anode ceramic matrix of $BaCe_{0.85}Y_{0.15}O_{2.925}$ (BCY15) is presented aiming to eliminate the problems associated with applying the traditional ceramic route for Ni/BCY cermet anode materials preparation. BCY15/Ni sample was synthesized by wet chemical reduction of Ni^{2+} ions with hydrazine hydrate ($N_2H_4 \cdot H_2O$) in an aqueous medium.

EXPERIMENTAL

Sample preparation

Nickel chloride hexahydrate ($NiCl_2 \cdot 6H_2O$), hydrazine monohydrate (99+% $N_2H_4 \cdot H_2O$), sodium hydroxide (NaOH) and anhydrous sodium carbonate (Na_2CO_3) of analytical grade procured by Alfa Aesar USA were used as received without further purification.

BCY15 powder (Marion Technology) was fabricated by auto-combustion process starting from metal nitrates and applying urea as reducing agent. Sintering of the precursor at 1100–1150°C in a carrier gas (helium or argon) for complete CO_2 elimination ensured the production of single phase powder with 48 % porosity, dominating particle size round 200 nm and minor degree of agglomeration. The powder was thermally pre-sintered at 1100°C for 2h before the anode cermet synthesis. The pre-sintering was associated with mass losses of about 0.7 wt. %.

BCY15/Ni sample with a composition of $NiO/BCY15 = 44.4/55.6$ (volume ratio) was synthesized in a five-necked glass reactor equipped with a steam jacket, stirrer, pH electrode, thermocouple and reflux condenser. An appropriate amount of $NiCl_2 \cdot 6H_2O$ was dissolved in deionized water, introduced in a reaction vessel and mixed with BCY15 powder in a quantity sufficient to satisfy the desired composition of the final compound. After stirring for a certain time, a suitable volume of 0.3M $N_2H_4 \cdot H_2O$ solution was slowly drop-wise introduced to the reactor by usage of peristaltic pump under vigorous stirring followed by addition of alkaline solution (3M NaOH/3M $Na_2CO_3 = 1/1$) in the same manner. The suspension was controlled heated up to 95°C at pH=12–13 under vigorous stirring. As the reduction reaction proceeded, green, blue, blue–violet or cyan colored Ni– N_2H_4 complexes $[Ni(N_2H_4)_n]Cl_2$ were initially generated, followed by transition to black, which indicated the formation of metal nickel. The reduction was accompanied by gaseous nitrogen evolution, followed by growth of Ni^0 particles on the BCY15 surface. After the reduction, the resulting mixture was stirred for 1 h at the selected pH and temperature. The obtained black material was filtrated and washed thoroughly with deionized water to remove the by-products of the filtrate which was indicated by decrease of pH down to 6.0. The absence of Cl^- ions was tested with aqueous solution of 1.5 % $AgNO_3$. The sample was further dried at 100°C for 20 h.

To get reference sample for the characterization of BCY15/Ni, unsupported nickel denoted as Ni, was prepared according to the preparation

procedure described above, however in the absence of the anode ceramic matrix BCY15.

Sample characterization

Powder X-ray diffraction (PXRD) data were collected on an APD 15 Philips 2134 diffractometer employing CuK radiation ($\lambda = 0.15418$ nm) operated at $U = 40$ kV and $I = 30$ mA. The crystalline phases were identified using Joint Committee on Powder Diffraction Standards (JCPDS) files. Electron microscope JEOL 6390 with INCA Oxford EDS detector was used for morphology observations.

The texture characteristics were determined by low-temperature (77.4 K) nitrogen adsorption in a Quantachrome Instruments NOVA 1200e (USA) apparatus. The nitrogen adsorption-desorption isotherms were analyzed to evaluate the specific surface area, determined on the basis of the BET equation. The pore-size distribution (PSD) was made by the adsorption branch of the isotherm using the method of Barrett-Joyner-Halenda. The samples were outgassed for 16 h in vacuum at 80°C before the measurements.

The electrochemical impedance measurements were performed on IVIUM - CompactStat e10030 in the temperature interval $100\text{--}750^\circ\text{C}$ and frequency range $1\text{ Hz--}0.01\text{ Hz}$ with density of 5 points/decade and amplitude of the AC signal 1 mA in reduction atmosphere.

RESULTS AND DISCUSSION

The PXRD patterns of BCY15 (Fig. 1a) show the presence of a single phase that can be attributed to orthorhombic perovskite, isostructural with BaCeO_3 (JCPDS file 00-022-0074) and yttrium doped analogue, $\text{BaCe}_{0.9}\text{Y}_{0.1}\text{O}_{2.95}$ (JCPDS file 01-081-1386). The recorded well-formed reflections of BaCeO_3 are in agreement with the calculated mean crystallite size (L) of $150.0(52)$ Å. No diffraction peaks due to Y_2O_3 phase are registered indicating that yttrium ions are incorporated into the perovskite lattice.

Applying PXRD data processing, the lattice parameters of BCY15 were evaluated and compared with those of standard JCPDS files for BaCeO_3 and $\text{BaCe}_{0.9}\text{Y}_{0.1}\text{O}_{2.95}$ (Table 1). The results obtained evidence similar values which are typical for O-type distorted perovskites. The deviation from the ideal perovskite structure can be ascribed to the distortion of the octahedra of the structure.

In general, the distortion of the ideal perovskite structure is manifested by sloping of the BO_6 octahedra, deformation of the BO_6 octahedra and displacement of the B-cation from the center of the

octahedra [21]. In the Y-doped BaCeO_3 the tilting of the octahedra decreases the ideal cubic symmetry to the orthorhombic O-type one.

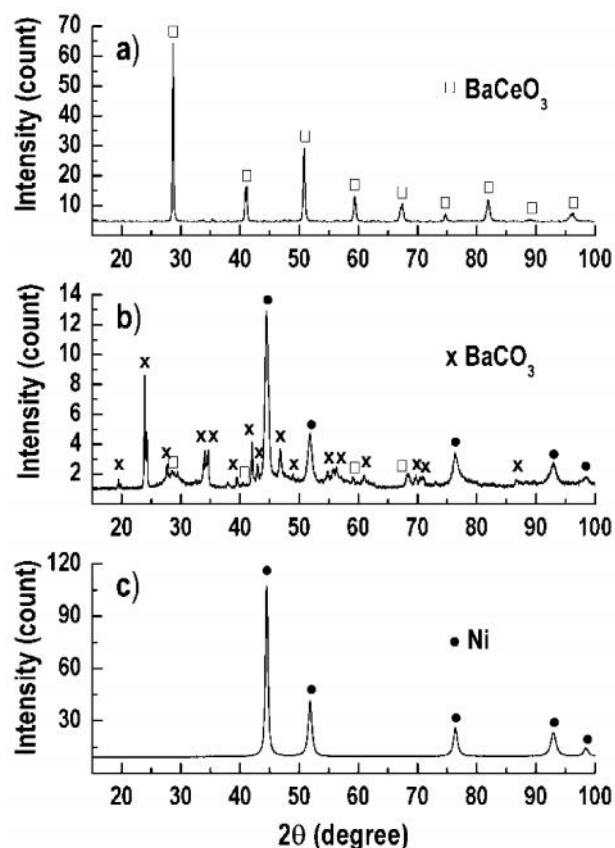


Fig. 1. XRD patterns of: (a) BCY15, (b) BCY15/Ni and (c) Ni samples.

The typical reflections of the metal Ni with cubic lattice symmetry (fcc) according to standard (JCPDS file 00-004-0085) and reference patterns of sample Ni (Fig. 1c) are clearly demonstrated in BCY15/Ni (Fig. 1b). The metal Ni lattice parameter (a) and the metal Ni cell volume (V_{cell}) of BCY15/Ni are presented in Table 2 showing values similar to those of standard metal Ni (JCPDS file 00-004-0850). A difference in the intensity of the metal Ni reflections going from BCY15/Ni to unsupported reference Ni sample is observed, indicating a different degree of crystallinity. This can be proved by estimating the mean metal Ni crystallite sizes (L) from the full-width at half-maximum values of the (111) diffraction lines (Table 2). Results display that the metal Ni crystallites created in BCY15/Ni (157 Å) are smaller than those in the unsupported reference sample Ni (190 Å), specifying the positive role of the BCY15 presence in the anode composite on the metal Ni dispersion.

Table 1. Iridium content in the test samples determined by EDX analysis and kinetic data assessing their catalytic activity.

Compound	JCPDS file	Unit cell parameters			
		a (Å)	b (Å)	c (Å)	V _{cell} (Å ³)
BCY15	-	8.7735(63)	6.2152(36)	6.2164(69)	338.97(38)
BaCeO ₃	00-022-0074	8.7790	6.2140	6.2360	340.19
BaCe _{0.9} Y _{0.1} O _{2.95}	01-081-1386	8.7705	6.2233	6.2393	340.55

Very well organized and intensive reflections of BaCO₃ phase with orthorhombic lattice symmetry (JCPDS file 00-045-1471) are also registered. The observed phenomenon proves that during the synthesis of BCY15/Ni, an interaction occurs between BCY15 and deionized water resulting in partial reorganization of the initial BCY15 structure as it can be expected due to the hydrophilic

properties of the ceramic matrix. The formation of BaCO₃ phase is related to the chemical instability of the BaCeO₃-based materials in a humid environment and the presence of CO₂, according to the reaction: BaCeO₃ + CO₂ → BaCO₃ + CeO₂. PXRD analysis discloses a small number of low intensity reflections of BaCeO₃ perovskite, most probably “covered” by the BaCO₃ phase.

Table 2. Lattice parameters of metal Ni and NiO obtained after treatment of Ni/BCY15 in different atmospheres.

Parameter	BCY15/Ni			Reference JCPDS files	
	as-prepared ^a	sintered ^b	reduced ^a	^a Ni ⁰ (00-004-0850)	^b NiO (00-047-1049)
a (Å)	3.5245(10)	4.1786(10)	3.5270(11)	3.5238	4.1771
V _{cell} (Å ³)	43.78(34)	72.96(55)	43.87(43)	43.76	72.88
L (Å)	157.0(41)	124.2(39)	231.0(22)	-	-

N₂-physisorption analysis reveals that BCY15 anode matrix represents typical macroporous material with Type II isotherm (Fig. 2a) that is characteristic of aggregated powders as clays, cements, etc. [22]. The observed very narrow hysteresis loop shows presence of some mesopores on the surface which are termed as Type IIb exhibiting Type H3 hysteresis. The character of the isotherm type is preserved after incorporation of Ni²⁺ ions subsequent by reduction to the metallic state (BCY15/Ni) with clearly outline hysteresis H3 Type, generated from the new mesopore system formation. Type H3 loop is given by aggregates of platy particles or adsorbents containing slit-shaped pores. The increase of surface area from 3 m²/g (BCY15) to 8 m²/g in BCY15/Ni confirms the creation of the new mesopore system. The pore size distribution (PSD) (Fig. 2b) illustrates uniform pore system for BCY15 powder and presence of macropores (above 50 nm). After the incorporation of Ni in BCY15, the PSD curve of BCY15/Ni takes a poly-dispersed character in the 3–20 nm area. The comparison with BCY15 matrix signifies a creation of new mesopores.

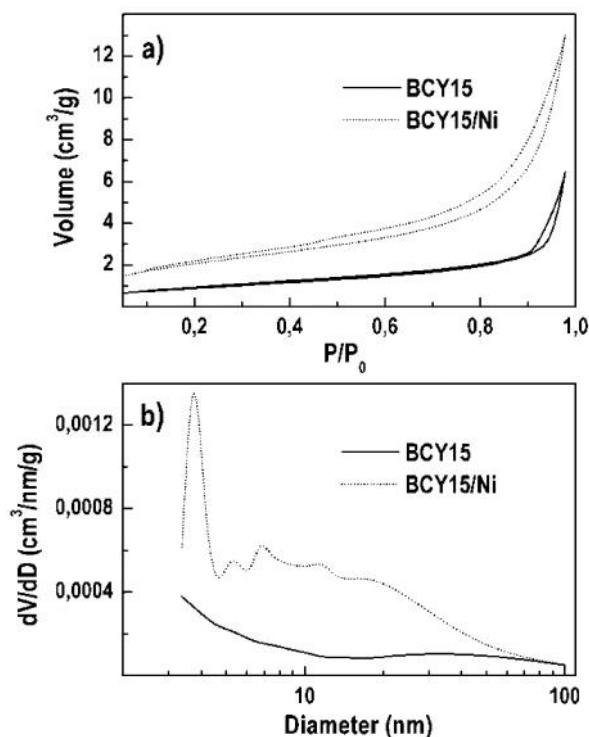


Fig. 2. N₂ sorption analysis of BCY15 and BCY15/Ni: (a) adsorption–desorption isotherms and (b) pore size distribution.

The value of BET parameter **C** increases from 90 for BCY15 to 97 for BCY15/Ni indicating an increase of adsorbent–adsorbate interaction in BCY15/Ni that may be assigned to the changes in the polarity of the surface as a result of the formation of mesoporous Ni-containing phase. Constant **C** is related to the interaction force of adsorbent–adsorbate [23].

SEM image of BCY15 powder reveals relatively homogeneous porous structure consisting of particles similar in kind and shape, randomly distributed on the surface (Fig. 3a).

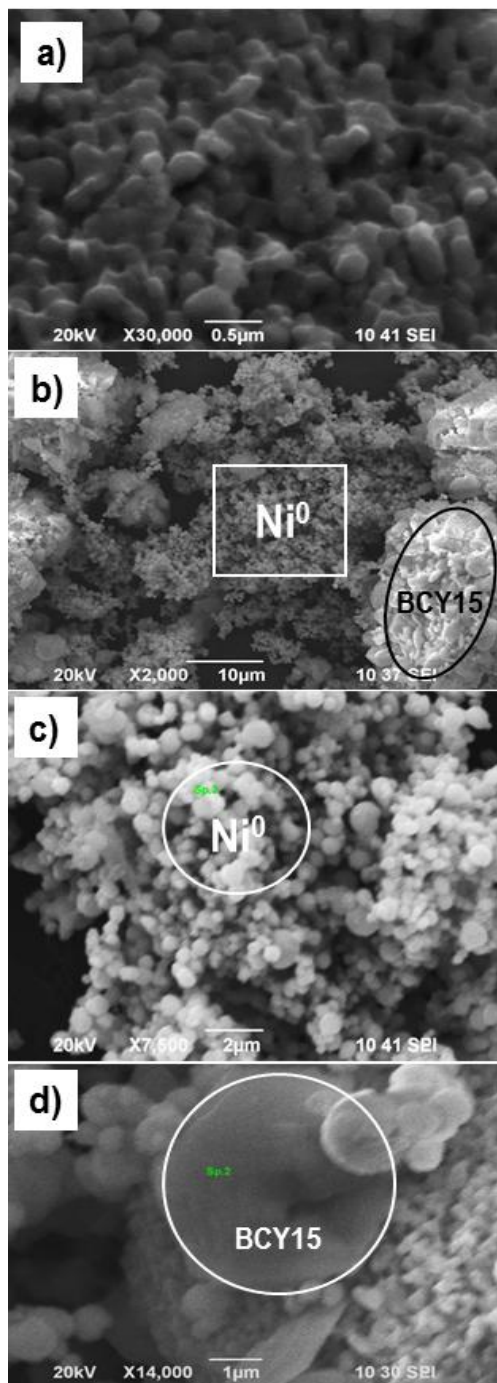


Fig. 3. Micrographs of BCY15 (a) and BCY15/Ni (b, c, d) solids.

The presented images of BCY15/Ni (Fig. 3b-d) illustrate change in the morphology of BCY15 ceramic matrix after nickel deposition. Fine mono-dispersed spherical metal nickel particles (Fig. 3b and c) along with fragments of BCY15 mixed or covered with angulated particles different in size can be easily identified on the surface of BCY15/Ni (Fig. 3b,d).

EDS surface composition analyses of BCY15 and BCY15/Ni are collected in Table 3. As it can be observed the composition of anode matrix is changed in a considerable extent after incorporation of metal nickel BCY15/Ni. The data testifies domains for metal nickel (Fig. 3c) and anode matrix (Fig. 3d) respectively, and confirms the results from PXRD analyses.

Table 3. EDS surface composition of BCY15 and BCY15/Ni.

Element (wt. %)	O	Ni	Ba	Ce	Y
BCY15	16.54	-	42.34	36.95	4.17
BCY15/ Ni*	14.83	76.38	5.93	2.86	0
BCY15/ Ni**	15.69	6.27	74.01	4.04	0

*from Fig. 3c; **from Fig. 3d

For analysis of the Ni network quality in a real anode, the standard ceramic technology was used for the preparation of pressed tablets from BCY15/Ni (cold pressing, 3t/5 min), followed by their sintering in air at 1200°C for 5 h. The volumetric shrinkage of the tablet was about 6%.

The thermal treatment of BCY15/Ni in air provokes an oxidation of the metal nickel phase to NiO. PXRD patterns (Fig. 4a) display reflections of well-organized NiO phase with lattice parameters (*a* and *V_{cell}*) close to the standard NiO (JCPDS file 00-047-1049) (Table 2). Well-defined reflections of BaCeO₃ phase can be detected, signifying partial recovery of the perovskite structure. Furthermore, an appearance of two poorly crystallized new phases is found, namely BaNiO_{2.36} with hexagonal crystal symmetry (JCPDS file 00-047-0089) and cubic Y_{0.10}Ce_{0.90}O_{1.95} (JCPDS file 01-075-0174). Consequently, the sintered product is a rather complex phase mixture.

After sintering, a step-wise standard reduction procedure was performed at 750°C for 5 h with a H₂/N₂ gaseous mixture to reduce NiO in the anode material to form BCY15/Ni composite. The first reduction step was accomplished with gaseous

mixture of N_2 (flow rate of $35 \text{ nml/min} \cdot \text{m}^{-2}$) and H_2 (flow rate of $10 \text{ nml/min} \cdot \text{m}^{-2}$) for 60 min. The second reduction step concerns treatment only with H_2 (flow rate of $35 \text{ nml/min} \cdot \text{m}^{-2}$) for 60 min.

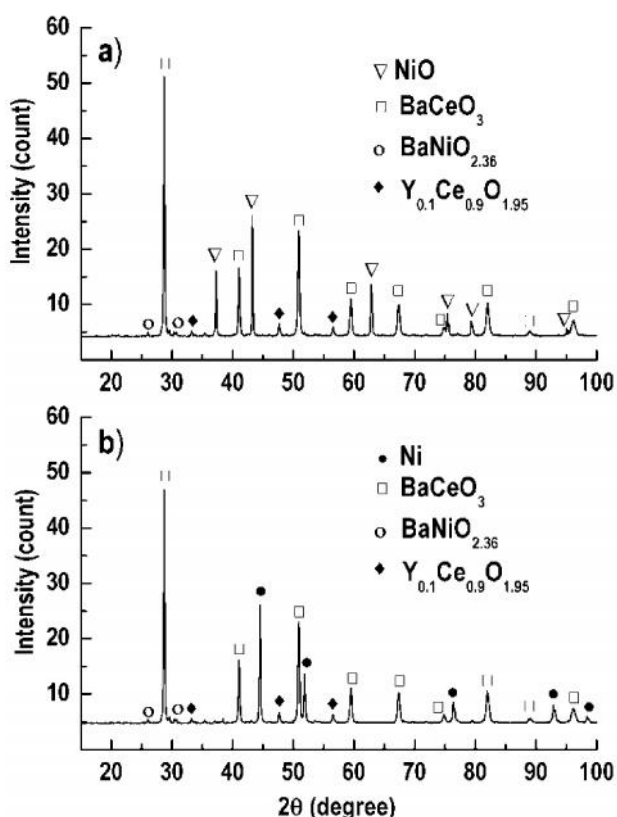


Fig. 4. XRD patterns of BCY15/Ni: (a) sintered and (b) reduced.

The PXRD analyses show that the reduction of sintered BCY15/Ni solid leads only to full conversion of NiO in the metal Ni state. Well organized reflections of metal Ni with cubic lattice symmetry are recorded (Fig. 4b) along with the $BaCeO_3$, $BaNiO_{2.36}$ and $Y_{0.10}Ce_{0.90}O_{1.95}$ phases. It may be summarized that the activation of the BCY15/Ni cermet by reduction with H_2 does not cause additional structural changes. The calculated metal Ni lattice parameters values (Table 2) are also comparable to those of the standard metal Ni (JCPDS file 00-004-0850). In addition, the reduction procedure causes growth of the metal Ni crystallites.

For *in situ* analysis of the Ni network performance a recently developed impedance approach for direct measurements of the Ni cermet electronic conductivity in the classical Ni-YSZ was applied [24]. The measurements are carried out directly on “bare” anodes sandwiched between two Ni contact nets. The direct analysis starts in the beginning of the reduction stage which was performed at 750°C . In this way, the electronic conductivity is directly measured giving

information about for the nickel network formation in the bulk anode structure.

The results obtained from the impedance measurements of BCY15/Ni anode cermet show that prior to the reduction, the cermet BCY15/Ni demonstrates a fairly low resistance of 31.5Ω (Fig. 5a), which suggests the presence of some percolation and indicates that the sintering procedure induces only partial oxidation of the metal Ni. The reduction proceeds quickly as the resistance of Ni net decreases down to $70 \text{ m}\Omega$ for about 20 min and this value remains unchanged until the end of the reduction cycle (Fig. 5b).

Similar phenomenon was observed in experiments with commercial YSZ/Ni cermet, namely Ni/YSZ produced by SOLIDpower (Fig. 5c).

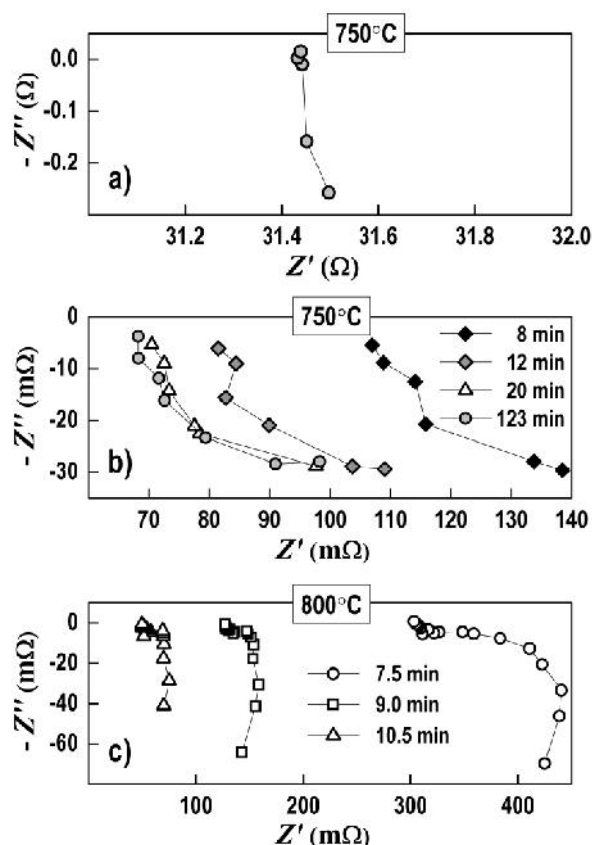


Fig. 5. Impedance diagrams of: () BCY15/Ni before the beginning of the reduction, (b) BCY15/Ni after 8, 12, 20 and 123 min reduction and () Ni/YSZ anode cermet (SOLIDpower) after 7.5, 9.0 and 10.5 min of reduction.

CONCLUSIONS

The results obtained in this study show that BCY15/Ni anode cermet demonstrated electrochemical performance similar to that of the commercial NiO-based anode cermets in respect to the electronic conductivity of the Ni net. The registered characteristics of BCY15/Ni anode

cermet make it suitable for application in BCY-based pSOFC.

The wet-chemical reduction route using hydrazine in an aqueous medium is a promising approach providing better conditions for nickel introduction in the anode ceramic matrix in comparison with the classical solid state ceramic approach.

The preparation of Ni/BCY15 in aqueous medium results in partial reorganization of the initial BCY15 structure due to the hydrophilic properties of the ceramic matrix. A fully preservation of the anode ceramic matrix in the Ni/BCY15 cermet may be achieved if the synthesis is performed in an anhydrous environment, which is the subject of our future investigations.

Acknowledgements: The research leading to these results has received funding from Bulgarian NSF under grant No E02/3/2014.

REFERENCES

1. A. Stambouli and E. Traversa, *Renew. Sust. Energ. Rev.*, **6**, 433 (2002).
2. R. Ormerod, *Chem. Soc. Rev.*, **32**, 17 (2003).
3. P. Frontera, V. Modafferi, F. Frusteri, G. Bonura, M. Bottari, S. Siracusano, P. Antonucci, *Int. J. Hydrogen Energy*, **35**, 11661 (2010).
4. A. Lapina, C. Chatzichristodoulou, P. Holtappels, M. Mogensen, *J. Electrochem. Soc.*, **161**, F833 (2014).
5. K. Knight, *Solid State Ionics*, **145**, 275 (2001).
6. E. Fabbri, D. Pergolesi, E. Traversa, *Chem. Soc. Rev.*, **39**, 4355 (2010).
7. H. Iwahara, *Solid State Ionics*, **77**, 289 (1995).
8. N. Ito, M. Iijima, K. Kimura, S. Iguchi, *J. Power Sources*, **152**, 200 (2005).
9. A. Essoumhi, G. Taillades, M. Taillades-Jacquín, D. Jones, J. Rozière, *Solid State Ionics*, **179**, 2155 (2008).
10. L. Chevallier, M. Zunic, V. Esposito, E. Di Bartolomeo, E. Traversa, *Solid State Ionics*, **180**, 715 (2009).
11. J. Dailly, M. Marrony, *J. Power Sources*, **240**, 323 (2013).
12. J. Dailly, M. Marrony, G. Taillades, M. Taillades-Jacquín, A. Grimaud, F. Mauvy, E. Louradour, J. Salmi, *J. Power Sources*, **255**, 302 (2014).
13. T. Higuchi, T. Owaku, Y. Iida, E. Sakai, M. Kobayashi, H. Kumigashira, *Solid State Ionics*, **270**, 1 (2015).
14. Y. Matsuzaki, I. Yasuda, *Solid State Ionics*, **152–153**, 463 (2002).
15. E. Fabbri, D. Pergolesi, E. Traversa, *Sci. Technol. Adv. Mater.*, **11** (2010) article 044301.
16. Q. Fu, F. Tietz, D. Sebold, S. Tao, J. Irvine, *J. Power Sources*, **171**, 663 (2007).
17. A. Safari, R. K. Panda, V. F. Janas, *Ferroelectricity. Materials, Characteristics, and Applications, Key Engineering Materials*, **122–124**, 35 (1996).
18. R.J. Bell, G.J. Millar, J. Drennan, *Solid State Ionics*, **131**, 211 (2000).
19. J. Park, E. Chae, S. Kim, J. Lee, J. Kim, S. Yoon, J.-Y. Choi, *Mater. Chem. Phys.*, **97**, 371 (2006).
20. G.-Y. Huang, S.-M. Xu, G. Xu, L.-Y. Li, L.-F. Zhang, *Trans. Nonferrous Met. Soc. China*, **19**, 389 (2009).
21. Budapest Neutron Centre, Progress report 2008–2009, Edited by R. Baranyai, M. Makai, L. Rosta, Budapest, September 2011; <http://www.bnc.hu>.
22. F. Rouquerol, J. Rouquerol, K. Sing, In *Adsorption by Powders and Porous Solids, Principle, Methodology and Applications*, Academic Press, New York, 1999.
23. A. Lecloux, J. Pirard, *J. Colloid Interf. Sci.*, **70**, 265 (1979).
24. D. E. Vladikova, Z. B. Stoyanov, Z. Wuillemin, D. Montinaro, P. Piccardo, I. Genov, M. Rolland, *ECS Transactions*, **68 (1)**, 1161 (2015).

Ni

I.

A

1*, 1, 2, 2, 1, 2

1, 11, 1113

10, 1113

2017 ; 11 2017 .

()

BaCe_{0.85}Y_{0.15}O_{2.925} (BCY15) ABO₃

BCY15/Ni

BCY15

BCY15/Ni

BCY15/Ni

Ni

NiO. BCY15/Ni BCY-

BCY15,